NACA

RESEARCH MEMORANDUM

AERODYNAMIC CHARACTERISTICS OF A WING WITH QUARTER-CHORD LINE SWEPT BACK 45°, ASPECT RATIO 6, TAPER RATIO 0.6, AND NACA 65A006 AIRFOIL SECTION

TRANSONIC-BUMP METHOD

By Kenneth W. Goodson and Albert G. Few, Jr.

Langley Aeronautical Laboratory
Langley Air Force Base, Va.

NATIONAL ADVISORY COMMITTEE
FOR AERONAUTICS

WASHINGTON

November 1, 1949

NACA RM L9I08

NATIONAL ADVISORY COMMITTEE FOR AERONAUTICS

RESEARCH MEMORANDUM

AERODYNAMIC CHARACTERISTICS OF A WING WITH QUARTER-CHORD LINE SWEPT BACK 45°, ASPECT RATIO 6, TAPER RATIO 0.6, AND NACA 65A006 AIRFOIL SECTION

TRANSONIC-BUMP METHOD

By Kenneth W. Goodson and Albert G. Few, Jr.

SUMMARY

As part of a transonic research program, a series of wings are being investigated in the Langley high-speed 7- by 10-foot tunnel over a Mach number range of about 0.60 to 1.18 by use of the transonic-bump test technique. In order to study the effects of wing geometry on the wing-alone and wing-fuselage longitudinal stability characteristics, the same fuselage is being used for all wings tested in this series.

This paper presents the results of the investigation of a wing-alone and a wing-fuselage configuration employing a wing with the quarter-chord line swept back 45°, aspect ratio 6, taper ratio 0.6, and an NACA 65A006 airfoil section. Lift, drag, pitching moment, and root bending moment were obtained for these configurations. In addition, effective downwash angles and dynamic-pressure characteristics in the region of the tail plane were also obtained for these configurations and are presented for a range of tail heights at one tail length. In order to expedite the publishing of these data, only a brief analysis is included.

INTRODUCTION

A series of wings are being investigated in the Langley high-speed 7- by 10-foot tunnel in order to study the effects of wing geometry on the wing-alone and wing-fuselage longitudinal stability characteristics at transonic speeds. The same fuselage is being used for all wings tested in this series. A Mach number range between 0.60 and 1.18 is obtained by use of the transonic-bump technique.

This paper presents the results of the investigation of the wing-alone and wing-fuselage configurations employing a wing with the quarter-chord line swept back 45°, aspect ratio 6, taper ratio 0.6, and an NACA 65A006 airfoil section parallel to the stream. Previous data published in this series for wings incorporating 45° sweepback can be obtained in references 1 and 2.

MODEL AND APPARATUS

The wing of the semispan model had 45° of sweepback referred to the quarter-chord line, aspect ratio 6, taper ratio 0.6, and an NACA 65A006 airfoil section parallel to the free stream. A two-view drawing of the model is presented in figure 1, and ordinates of the fuselage of fineness ratio 10 are given in table I. The wing was made of steel and the fuselage of brass.

The model was mounted on an electrical strain-gage balance which was enclosed in the bump. The lift, drag, pitching moment, and bending moment were measured with a strain-gage balance.

Effective downwash angles were determined for a range of tail heights by measuring the floating angles of five geometrically similar free-floating tails with the aid of calibrated slide-wire potentiometers. Details of the floating tails are shown in figures 2 and 3, and a photograph of the model on the bump with three of the floating tails is given as figure 4. The tails used in this investigation were the same as those used in references 1 and 2. A cutaway view of the sponge-wiper seal installed on the model is shown in figure 5.

A total-pressure rake was used to determine point dynamic-pressure ratios for a range of tail heights in a plane which contained the 25-percent mean-aerodynamic-chord point of the free-floating tails. The total-pressure tubes were spaced 1/8 inch apart near the wing chord line extended and 1/4 inch apart elsewhere.

COEFFICIENTS AND SYMBOLS

C_L lift coefficient $\left(\frac{\text{Twice panel lift}}{qS}\right)$

C_D drag coefficient $\left(\frac{\text{Twice panel drag}}{qS}\right)$

[redacted]

C_m pitching-moment coefficient referred to $0.25\bar{c}$ $\left(\frac{\text{Twice panel pitching moment}}{qS\bar{c}}\right)$

C_B bending-moment coefficient at plane of symmetry $\left(\frac{\text{Root bending moment}}{q\frac{S}{2}\frac{b}{2}}\right)$

q effective dynamic pressure over span of model, pounds per square foot $\left(\frac{1}{2}\rho V^2\right)$

q_a average chordwise local dynamic pressure, pounds per square foot

S twice wing area of semispan model, 0.125 square foot

$\bar{c}$ mean aerodynamic chord of wing, 0.147 foot; based on relationship $\frac{2}{S}\int_0^{b/2} c^2 dy$ (using theoretical tip)

$\bar{c}_t$ mean aerodynamic chord of tail

c local wing chord

b twice span of semispan model

y spanwise distance from plane of symmetry

ρ air density, slugs per cubic foot

V free-stream velocity, feet per second

M effective Mach number over span of model

M_l local Mach number

M_a average chordwise local Mach number

R Reynolds number of wing based on $\bar{c}$

α angle of attack, degrees

ϵ effective downwash angle, degrees

[redacted]

$\frac{q_{wake}}{q}$ ratio of point dynamic pressure at the quarter chord of the tail mean aerodynamic chord to free-stream dynamic pressure at the tail

y_{cp} lateral center of pressure, percent semispan $\left(100 \frac{C_B}{C_L}\right)$

h_t tail height relative to wing chord plane extended, percent wing semispan; positive for tail positions above chord plane extended

TESTS

The tests were made in the Langley high-speed 7- by 10-foot tunnel by use of an adaptation of the NACA wing-flow technique for obtaining transonic speeds. The technique used involves the mounting of a model in the high-velocity flow field generated over the curved surface of a bump located on the tunnel floor. (See reference 3.)

Typical contours of local Mach number in the vicinity of the model location on the bump, obtained from surveys with no model in position, are shown in figure 6. It is seen that there is a Mach number variation of about 0.05 over the model semispan at the lowest Mach numbers and from 0.08 to 0.09 at the highest Mach numbers. The chordwise Mach number variation is generally less than 0.01. No attempt has been made to evaluate the effects of the chordwise and spanwise Mach number variation. Note that the long dashed lines shown near the root of the wing (fig. 6) represent a local Mach number that is 5 percent below the maximum value and indicate the extent of the bump boundary layer. The effective test Mach number was obtained from contour charts similar to those presented in figure 6 by use of the relationship

$$M = \frac{2}{S} \int_0^{b/2} c M_a dy$$

Similarly, the effective dynamic pressure was determined from dynamic-pressure contour charts by using the relation

$$q = \frac{2}{S} \int_0^{b/2} c q_a dy$$

The variation of mean test Reynolds number with Mach number is shown in figure 7. The boundaries on the figure indicate the range in Reynolds number caused by variations in atmospheric test conditions in the course of the investigation.

Force and moment data, effective downwash angles, and the ratio of dynamic pressure at 25 percent of the mean aerodynamic chord of the tail to free-stream dynamic pressure at the tail were obtained for the model configurations tested through a Mach number range of 0.60 to 1.18 and an angle-of-attack range of -2° to 10°.

The end-plate tare corrections to the drag and to the downwash data were obtained through the test Mach number range at an angle of attack of 0° by testing the model configurations without end plates. A gap of about 1/16 inch was maintained between the wing root chord and the bump surface, and a sponge-wiper seal (fig. 5) was fastened to the wing butt beneath the surface of the bump to minimize leakage. The end-plate tares were found to be constant with angle of attack and the tares obtained at zero angle of attack were applied to all drag and downwash data. Jet-boundary corrections have not been evaluated because the boundary conditions to be satisfied are not rigorously defined. However, inasmuch as the effective flow field is large compared with the span and chord of the model, the corrections are believed to be small. No base pressure correction has been applied to the wing-fuselage drag data.

By measurements of tail floating angles without a model installed, it was determined that a tail spacing of 2 inches would produce negligible interference effects of reflected shock waves on the tail floating angles. Downwash angles for the wing-alone configuration were therefore obtained simultaneously for the middle, highest, and lowest tail positions in one series of tests and simultaneously for the two intermediate positions in succeeding runs. (See fig. 3.) Excluding the middle tail, the same procedure was used to determine the effective downwash angles for the wing-fuselage configuration. In order to obtain downwash data for the chord-plane-extended position, a series of tests were run with a free-floating tail mounted on the center line of the fuselage. The downwash angles presented are increments from the tail floating angles without a model in position. It should be noted that the floating angles measured are in reality a measure of the angle of zero pitching moment about the tail-pivot axis rather than the angle of zero lift. It has been estimated that, for this tail arrangement, an arbitrary downwash gradient as large as 2° across the span of the tail would result in an error within the experimental accuracy of the measured downwash angle.

[redacted]

The total-pressure readings in the tail plane were obtained at constant angles of attack through the Mach number range without an end plate on the model to eliminate end-plate wakes and with the support strut gap sealed with a rubber-sponge-type seal to minimize any strut leakage effects. The static-pressure values used in computing dynamic-pressure ratios were obtained by use of a static probe with no model in position.

RESULTS AND DISCUSSION

A table of the figures presenting the results follows:

	Figure
Wing-alone force data	8
Wing-fuselage force data	9
Effective downwash angles (wing alone)	10
Effective downwash angles (wing fuselage)	11
Downwash gradients	12
Dynamic-pressure surveys	13
Summary of aerodynamic characteristics	14
Effect of aspect ratio on minimum drag	15

Unless otherwise noted, the discussion is based on the summary curves presented in figure 14. The slopes presented in this figure have been averaged over a lift-coefficient range of ±0.1 of the specified lift coefficient.

Lift and Drag Characteristics

The wing-alone lift-curve slope measured near zero lift was about 0.059 at a Mach number of 0.60. This slope compares with a value of 0.062 estimated for this Mach number using unpublished semi-span data for a geometrically similar model from the Langley two-dimensional low-turbulence tunnel ($R = 1.5 \times 10^6$ to 6.0×10^6) as a low-speed point and applying a compressibility correction as outlined in reference 4. The lift-curve slope is practically invariant with Mach number below force break. At $M = 0.90$ the wing-alone lift-curve slope was about 0.061 as compared with 0.066 obtained at this same Mach number for the 45° sweptback wing of aspect ratio 4 and taper ratio 0.6. (See reference 1.) The addition of the fuselage increased the lift-curve slope near zero lift approximately 15 to 25 percent through the test Mach number range.

[redacted]

The drag-rise Mach number at zero lift is not clearly defined for the wing-alone configuration, although the initial drag rise would appear to occur in the neighborhood of $M = 0.90$. The drag-rise Mach number for the wing-fuselage configuration was about 0.94. The drag data for the 45° sweptback wing of aspect ratio 4 published in reference 1 are not directly comparable with the present results because drag data of reference 1 were not corrected for end-plate tares. Subsequent to the issuance of reference 1, however, drag data were obtained for the wing of reference 1 by use of the sponge-wiper seal technique previously mentioned in this paper. These data are presented in figure 15 together with a comparison with the wing of aspect ratio 6 of this paper. The wing-alone data (fig. 15) show that the effect of aspect ratio is negligible at Mach numbers below 1.05. However, at a Mach number of 1.15, the wing of aspect ratio 6 had a drag value 0.009 higher than the wing of aspect ratio 4. A similar increase in drag with increase in aspect ratio at the highest Mach numbers was obtained for the wing-fuselage configuration.

The lateral center of pressure y_{cp} for the wing alone was located at about 45 percent of the semispan at Mach numbers from 0.60 to 0.95 and at lift coefficients below 0.2. The same y_{cp} was obtained at low speeds from the aforementioned Langley two-dimensional low-turbulence tunnel tests of a geometrically similar wing for a higher Reynolds number range (between 3×10^6 to 6×10^6); however, at a Reynolds number of 1.5×10^6, y_{cp} was located several percent further outboard. The results of the present tests show that, between $M = 0.95$ and 1.00, y_{cp} moved inboard to about 42.5 percent of the semispan and remained constant up to $M = 1.18$. The addition of the fuselage shifted y_{cp} inboard about 1 percent up to $M = 1.00$ but had no effect at higher Mach numbers.

Pitching-Moment Characteristics

Near zero lift the wing-alone aerodynamic center was located at 39 percent mean aerodynamic chord in the Mach number range from 0.60 to 0.85. The unpublished data of the Langley two-dimensional low-turbulence tunnel on a geometrically similar wing indicated an aerodynamic-center position of 25 percent mean aerodynamic chord. In general, the position of the wing-alone aerodynamic center obtained at Mach numbers of about 0.60 in this series of bump investigations has indicated a somewhat more rearward aerodynamic-center position on wings of appreciable sweepback than that obtained from comparable low-speed data of the Langley two-dimensional low-turbulence tunnel. (See references 1, 2, and 5.) This aerodynamic-center shift may be

[redacted]

attributed to the low Reynolds numbers of the bump investigations. At the highest Mach numbers (1.05 to 1.18) there is a distinct flat spot in the C_m curves near zero lift (fig. 8) corresponding to an appreciable forward shift in aerodynamic-center location. Similar flat spots were evident from the data of reference 1. The addition of the fuselage moved the aerodynamic center forward about 8 percent mean aerodynamic chord at low Mach numbers. However, for Mach numbers between 1.00 and 1.10 the addition of the fuselage increased the stability. The large increase in stability contributed by the fuselage was associated with the delayed appearance of flat spots in the C_m curves to a higher Mach number. At the highest Mach number reached, these flat spots appear in both sets of data.

In the subsonic speed range, the wing-alone and wing-fuselage C_m curves indicate appreciable instability at the higher lift coefficients. (See figs. 8, 9, and 14.) This instability which is characteristic of wings with appreciable sweepback occurred at the same C_L but appeared to be considerably more pronounced than was shown in the data of the wing of aspect ratio 4 (reference 1). At the higher Mach numbers this instability appeared to be delayed to a much higher lift coefficient. Similar effects at Mach numbers above unity were also shown in references 1 and 2.

Downwash and Dynamic-Pressure Surveys

The downwash gradient $\partial\epsilon/\partial\alpha$ near zero lift for both the wing-alone and wing-fuselage configurations generally was a maximum near the wing chord plane extended although the variation with tail height was quite small in the range investigated. (See fig. 12.) The variation of $\partial\epsilon/\partial\alpha$ with Mach number for $h_t = 0$ and ± 30 percent wing semispan indicated an appreciable decrease in the downwash gradients at the highest Mach numbers, particularly for the wing-fuselage configuration (fig. 14).

The results of point dynamic-pressure surveys are presented in figure 13. There is very little change in wake characteristics as the Mach number is increased to 1.15, and the addition of the fuselage had practically no effect on the dynamic-pressure ratios through the Mach number range.

Langley Aeronautical Laboratory
National Advisory Committee for Aeronautics
Langley Air Force Base, Va.

[redacted]

REFERENCES

1. Weil, Joseph, and Goodson, Kenneth W.: Aerodynamic Characteristics of a Wing with Quarter-Chord Line Swept Back 45°, Aspect Ratio 4, Taper Ratio 0.6, and an NACA 65A006 Airfoil Section. Transonic-Bump Method. NACA RM L9A21, 1949.

2. Myers, Boyd C., II, and King, Thomas J., Jr.: Aerodynamic Characteristics of a Wing with Quarter-Chord Line Swept Back 45°, Aspect Ratio 4, Taper Ratio 0.3, and NACA 65A006 Airfoil Section. Transonic-Bump Method. NACA RM L9E25, 1949.

3. Schneiter, Leslie E., and Ziff, Howard L.: Preliminary Investigation of Spoiler Lateral Control on a 42° Sweptback Wing at Transonic Speeds. NACA RM L7F19, 1947.

4. DeYoung, John: Theoretical Additional Span Loading Characteristics of Wings with Arbitrary Sweep, Aspect Ratio, and Taper Ratio. NACA TN 1491, 1947.

5. King, Thomas J., Jr., and Myers, Boyd C., II: Aerodynamic Characteristics of a Wing with Quarter-Chord Line Swept Back 60°, Aspect Ratio 4, Taper Ratio 0.6, and NACA 65A006 Airfoil Section. Transonic-Bump Method. NACA RM L9G27, 1949.

[redacted]

TABLE I.- FUSELAGE ORDINATES

Basic fineness ratio 12; actual fineness ratio 10 achieved by cutting off the rear one-sixth of the body; $\bar{c}/4$ located at $l/2$

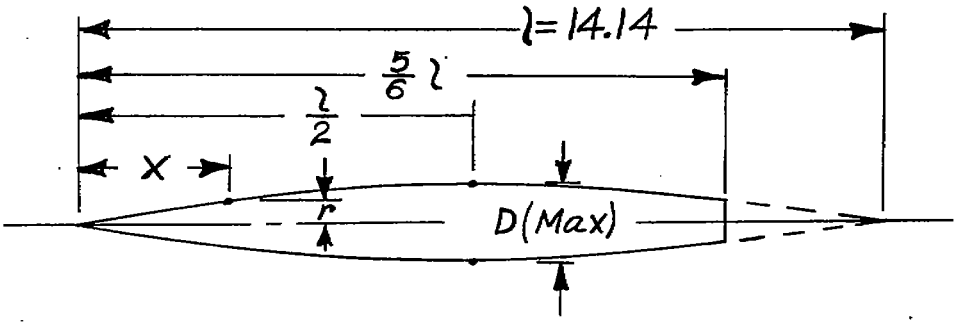

Ordinates			
x/l	r/l	x/l	r/l
0	0	0	0
.005	.00231	.4500	.04143
.0075	.00298	.5000	.04167
.0125	.00428	.5500	.04130
.0250	.00722	.6000	.04024
.0500	.01205	.6500	.03842
.0750	.01613	.7000	.03562
.1000	.01971	.7500	.03128
.1500	.02593	.8000	.02526
.2000	.03090	.8338	.02000
.2500	.03465	.8500	.01852
.3000	.03741	.9000	.01125
.3500	.03933	.9500	.00439
.4000	.04063	1.0000	0
L. E. radius = 0.0005l			

NACA

[redacted]

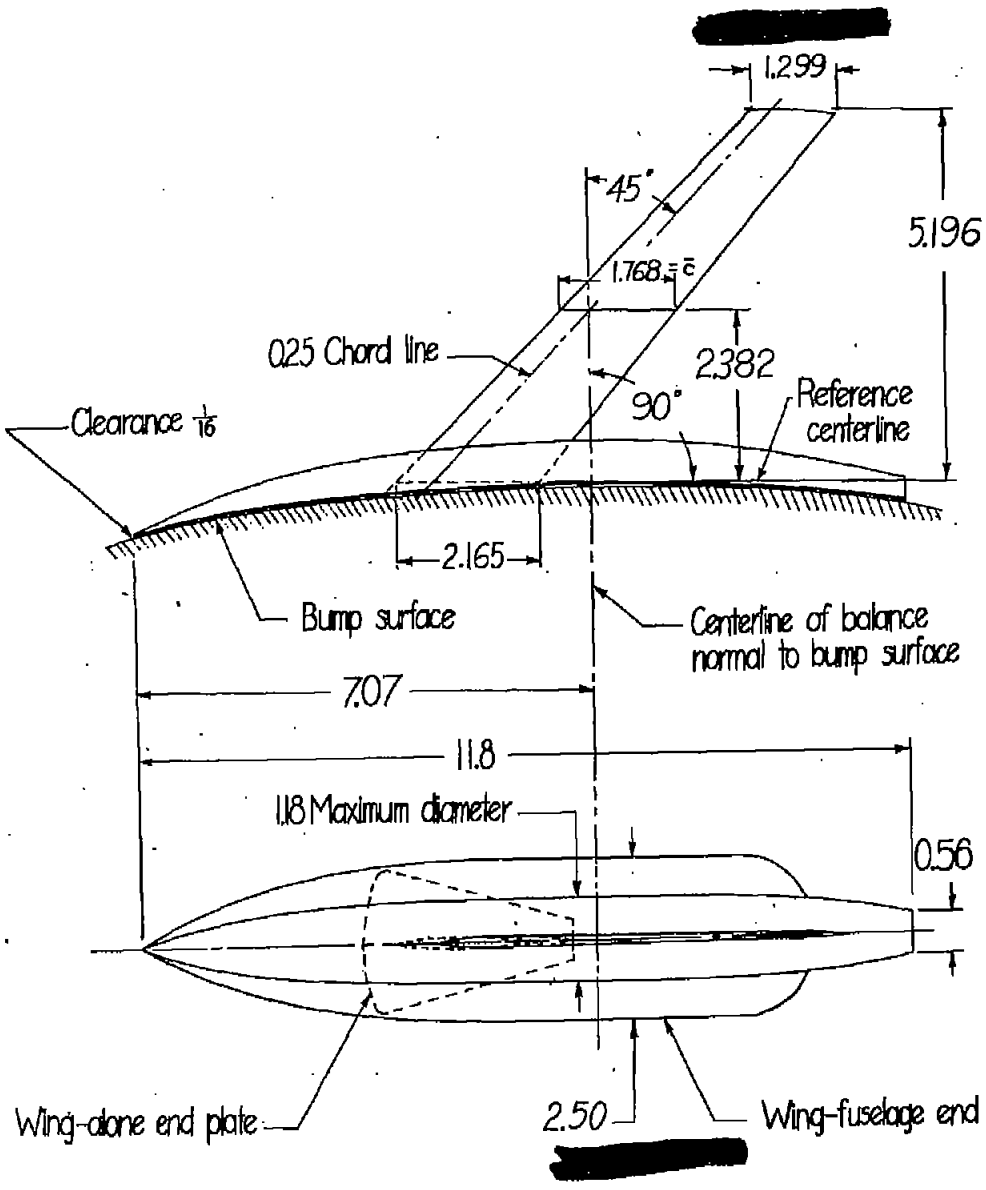

Tabulated Wing Data

Area (Twice semispan)	0.125 sq ft
Mean aerodynamic chord	0.1473 ft
Aspect ratio	6
Taper ratio	0.6
Incidence	0.0°
Dihedral	0.0°
Airfoil section parallel to free stream	NACA 65A006

0 1 2
Scale, inches

NACA

Figure 1.– General arrangement of a model with 45° sweptback wing, aspect ratio 6, taper ratio 0.6, and NACA 65A006 airfoil section.

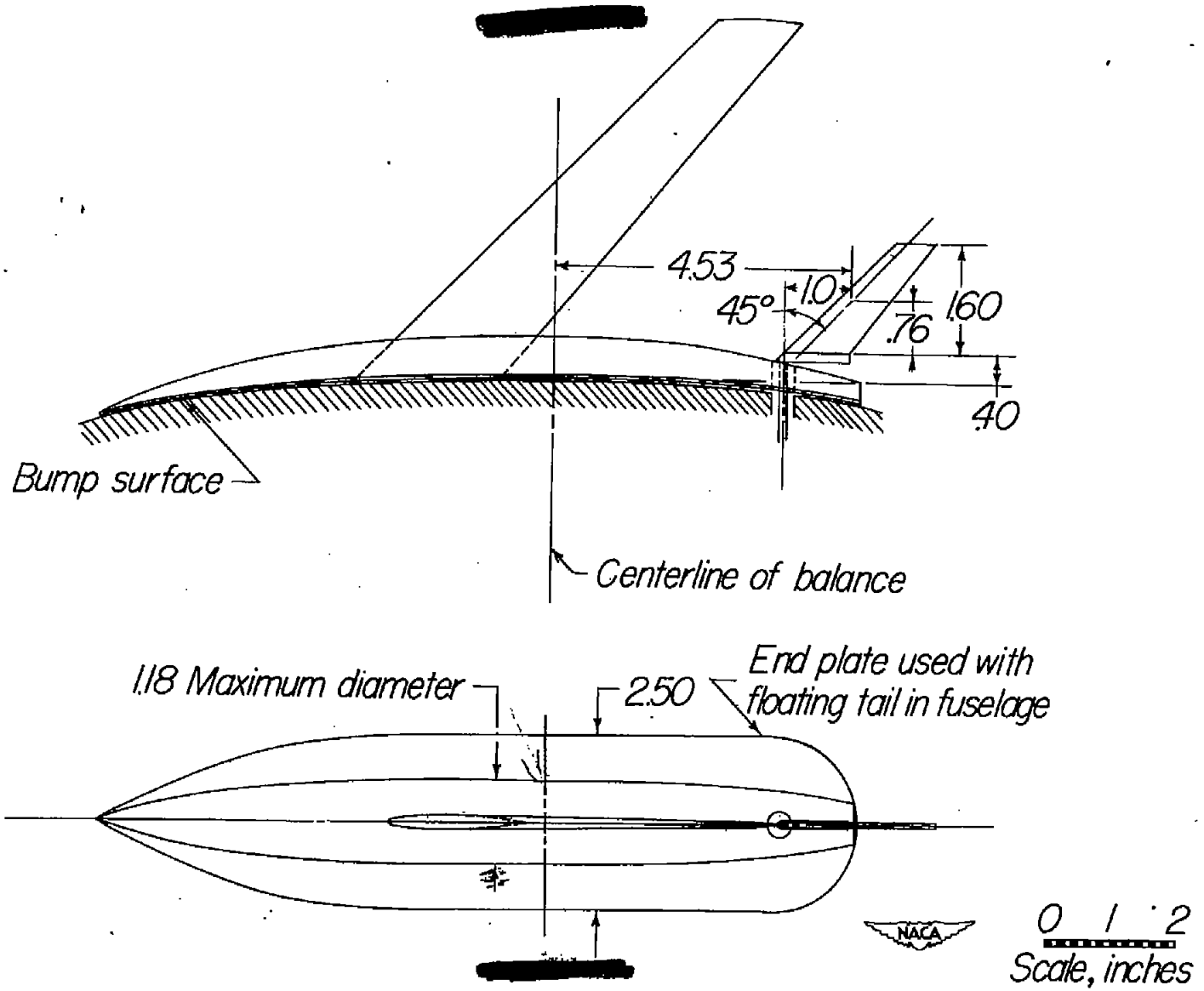

Figure 2.– Details of free-floating tail mounted in fuselage of a model with 45° sweptback wing, aspect ratio 6, taper ratio 0.6, and NACA 65A006 airfoil section.

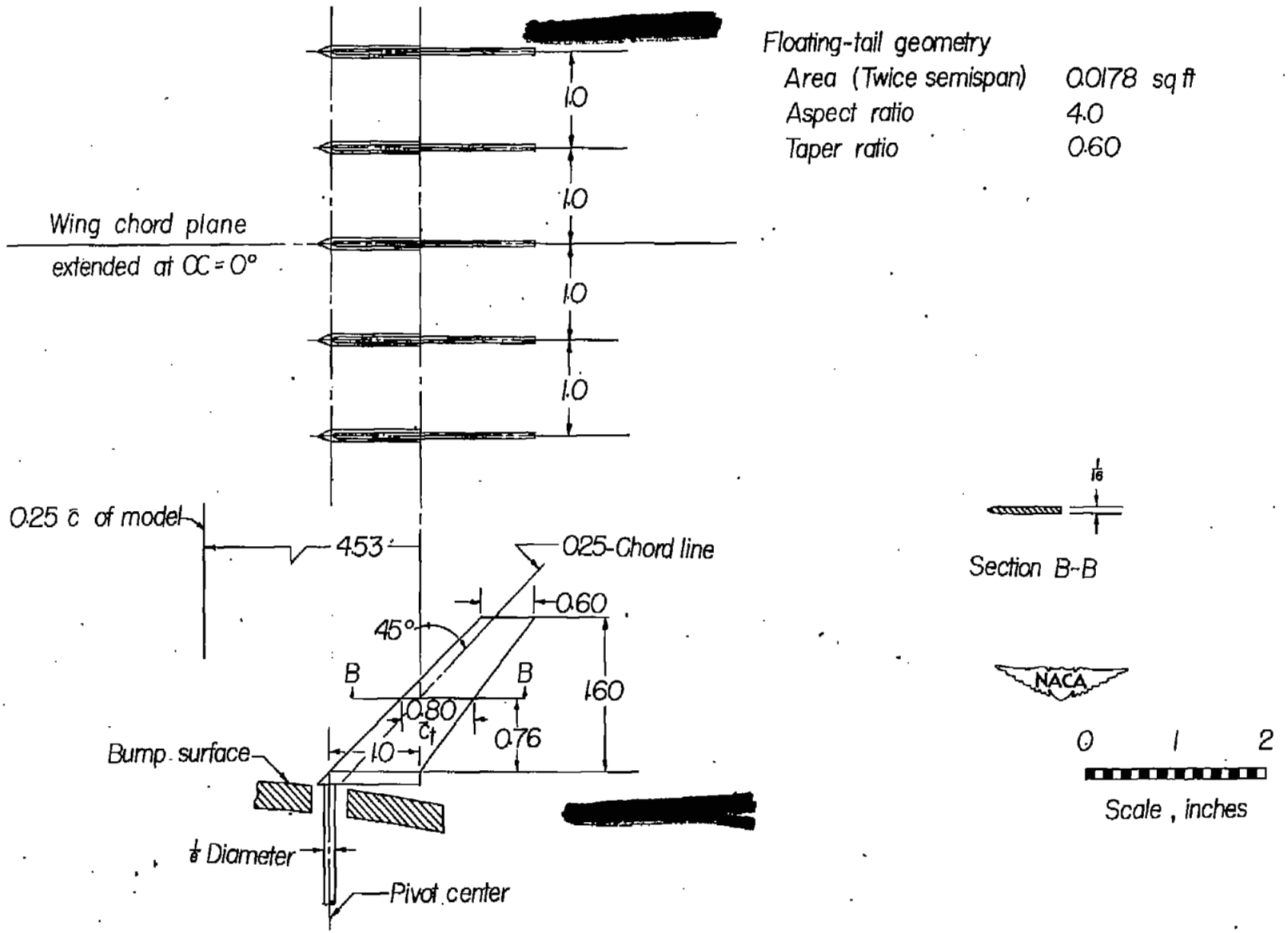

Figure 3.– Details of free-floating tails used in surveys behind model with 45° sweptback wing, aspect ratio 6, taper ratio 0.6, and NACA 65A006 airfoil section.

Figure 4.– Photograph of a model with 45° sweptback wing, aspect ratio 6, taper ratio 0.6, and NACA 65A006 airfoil mounted on the bump.

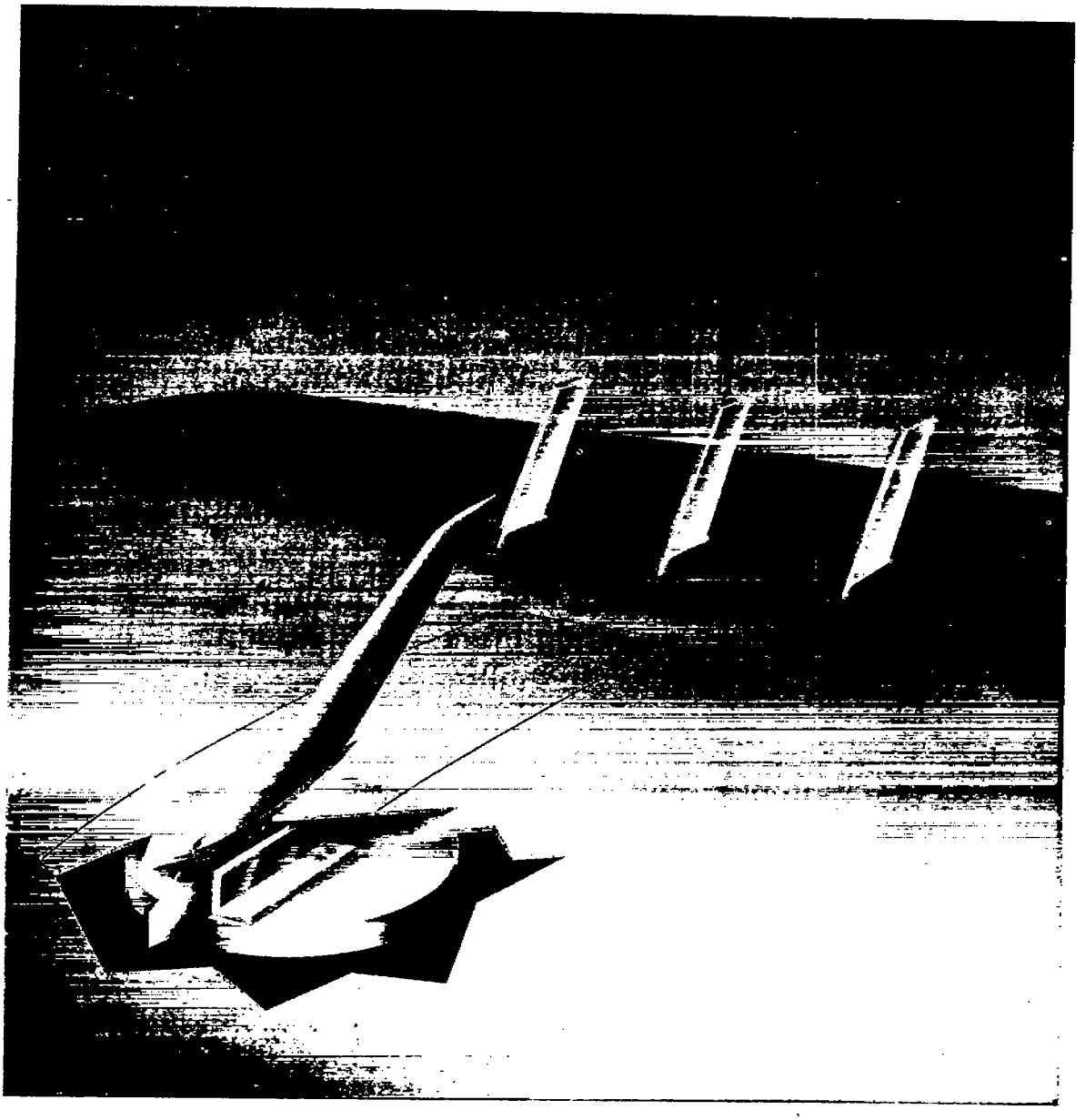

NACA

L-61938

Figure 5.— A cutaway view showing the sponge-wiper seal installation on the model with 45° sweptback wing, aspect ratio 6, taper ratio 0.6, and NACA 65A006 airfoil section.

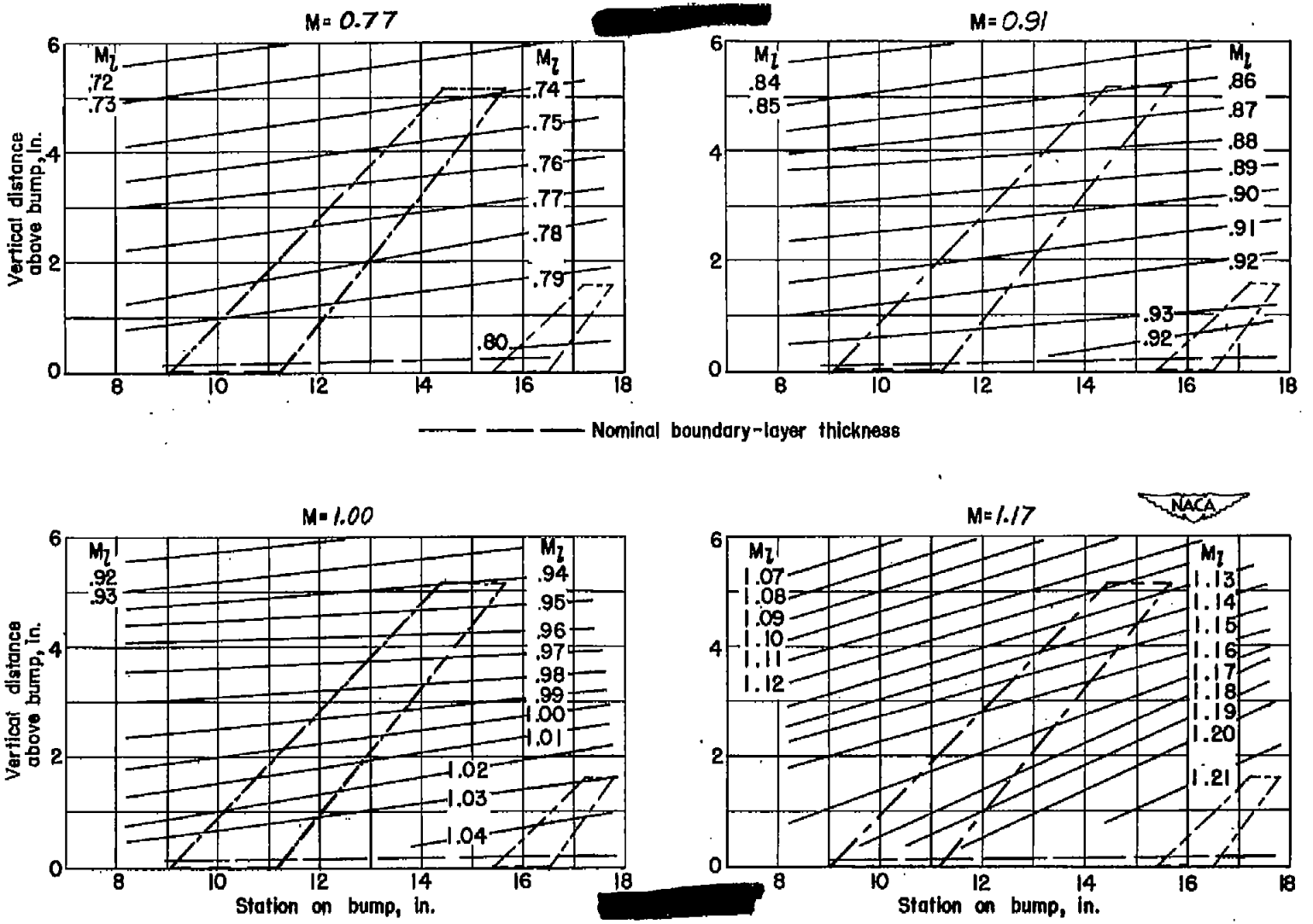

Figure 6.– Typical Mach number contours over transonic bump in region of model location.

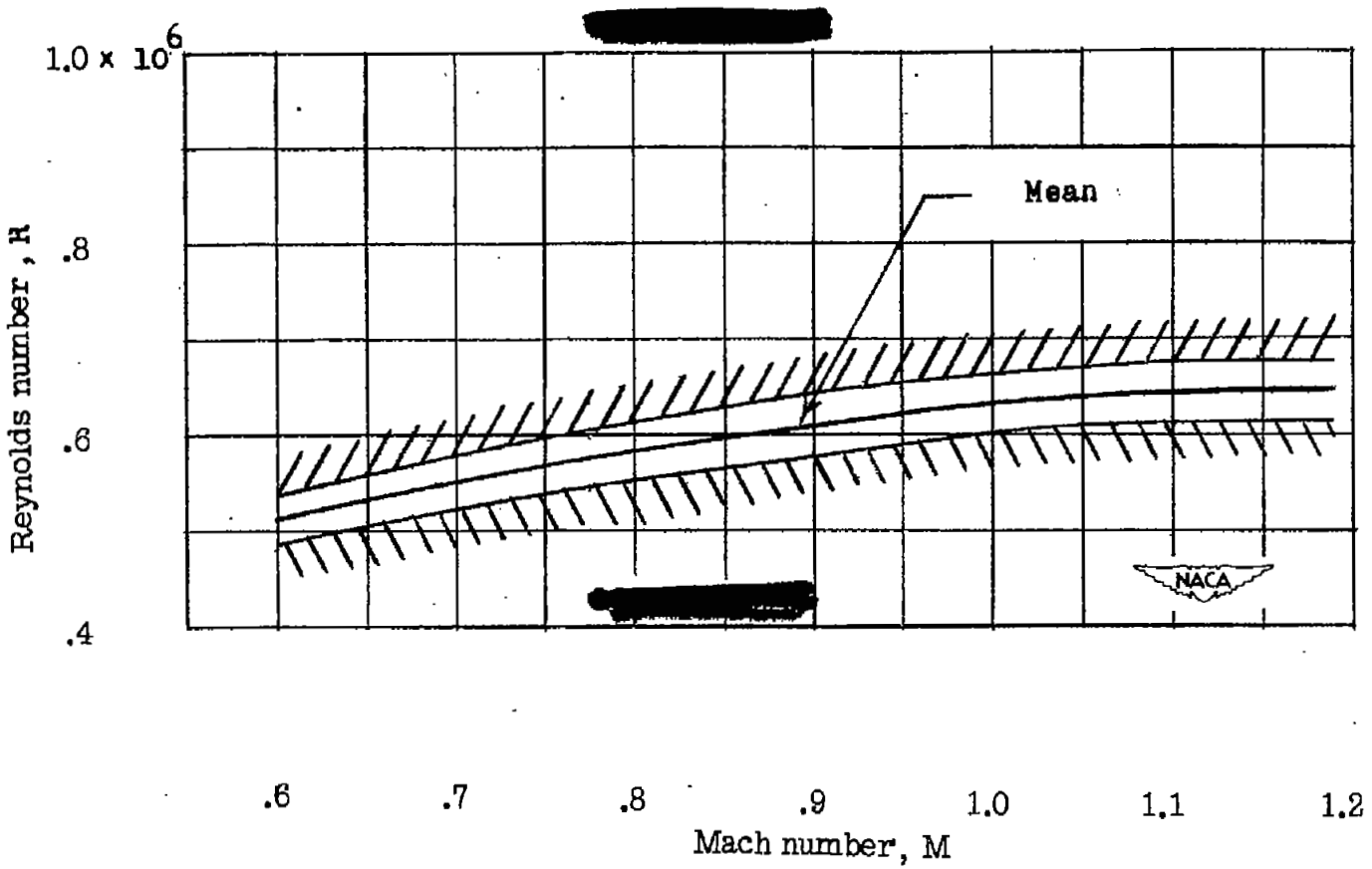

Figure 7.– Variation of test Reynolds number with Mach number for a model with 45° sweptback wing, aspect ratio 6, taper ratio 0.6, and NACA 65A006 airfoil section.

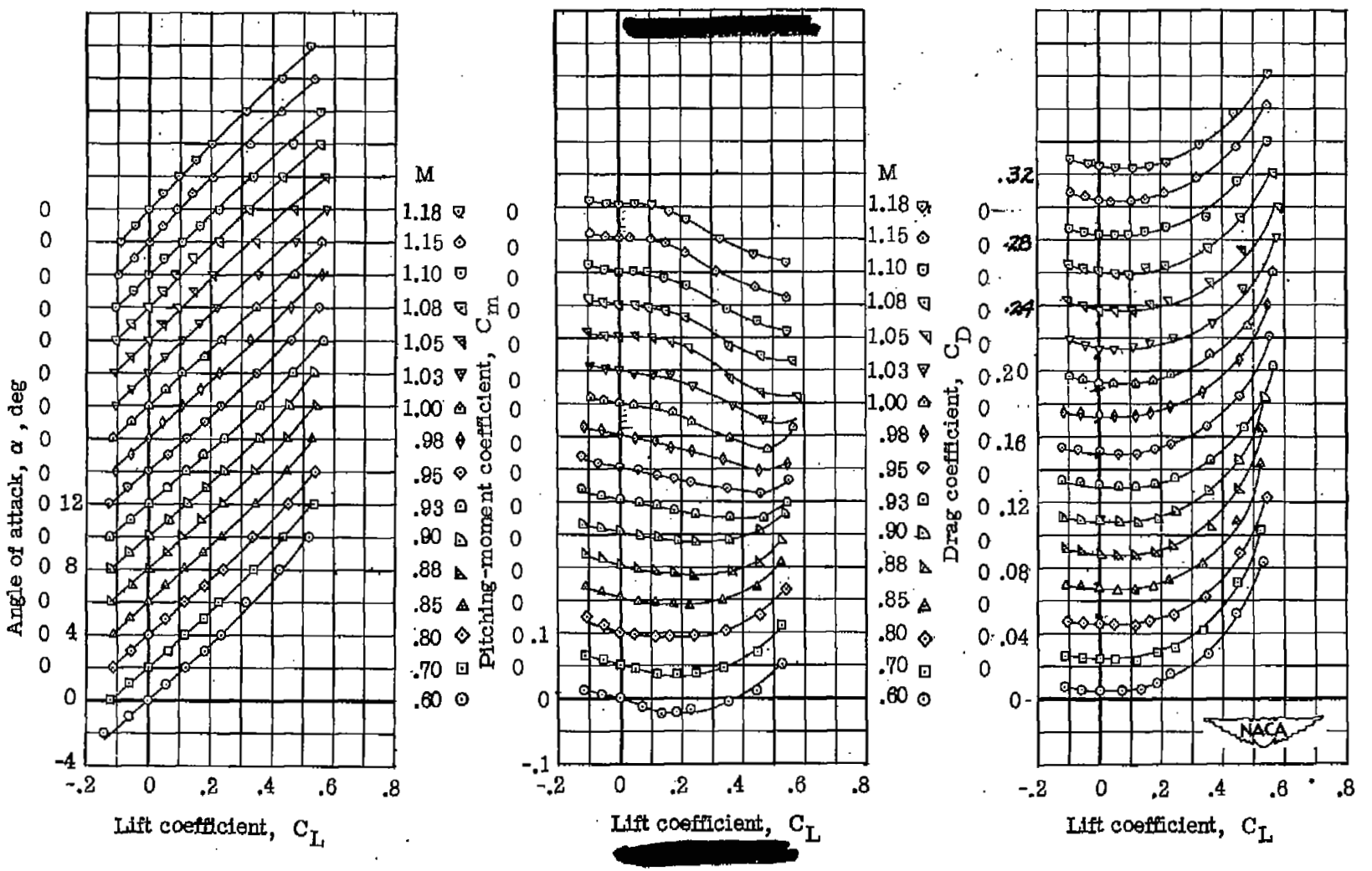

Figure 8.– Aerodynamic characteristics for a model with 45° sweptback wing, aspect ratio 6, taper ratio 0.6, and NACA 65A006 airfoil section. Wing alone.

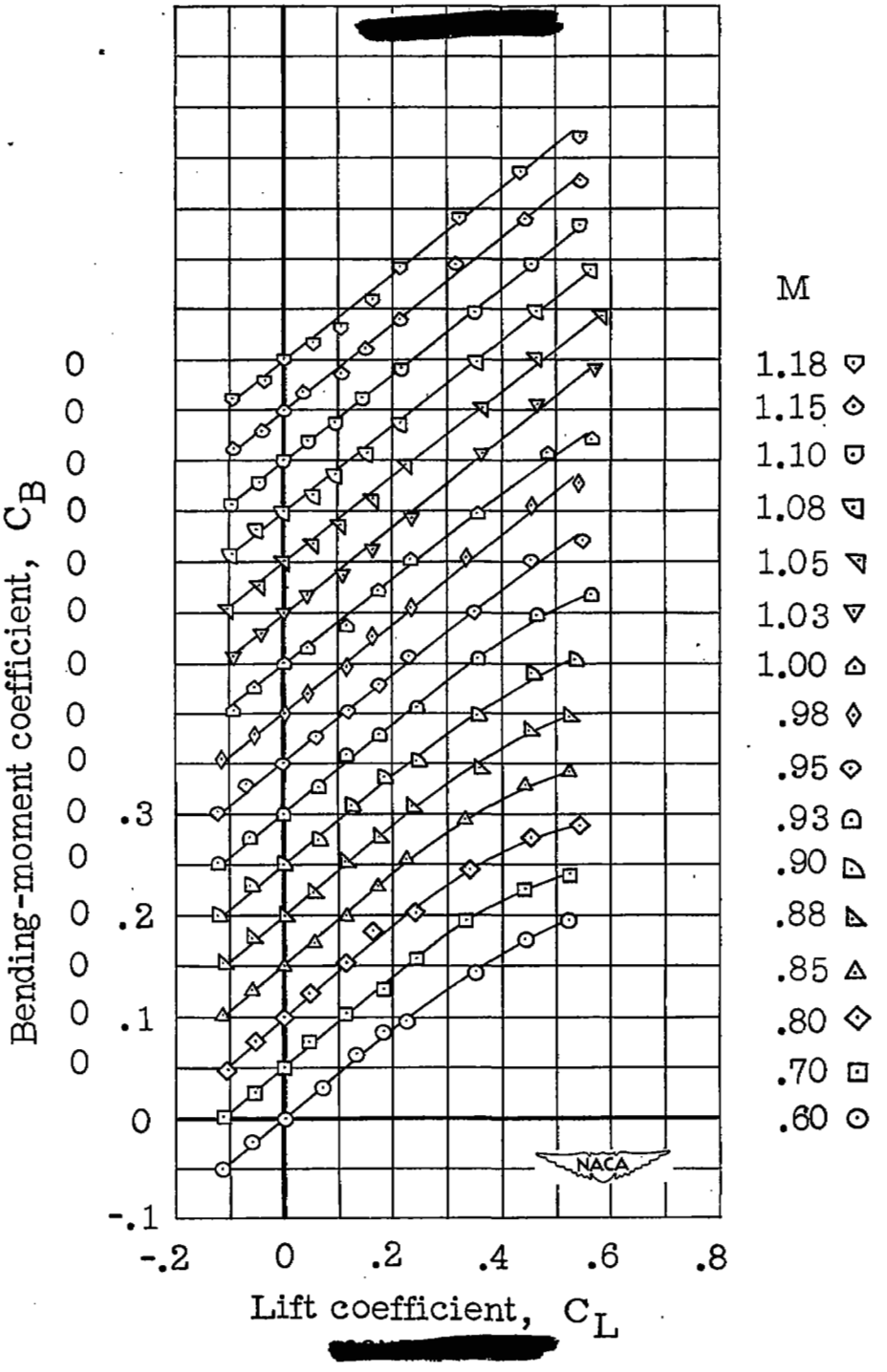

Figure 8.— Concluded.

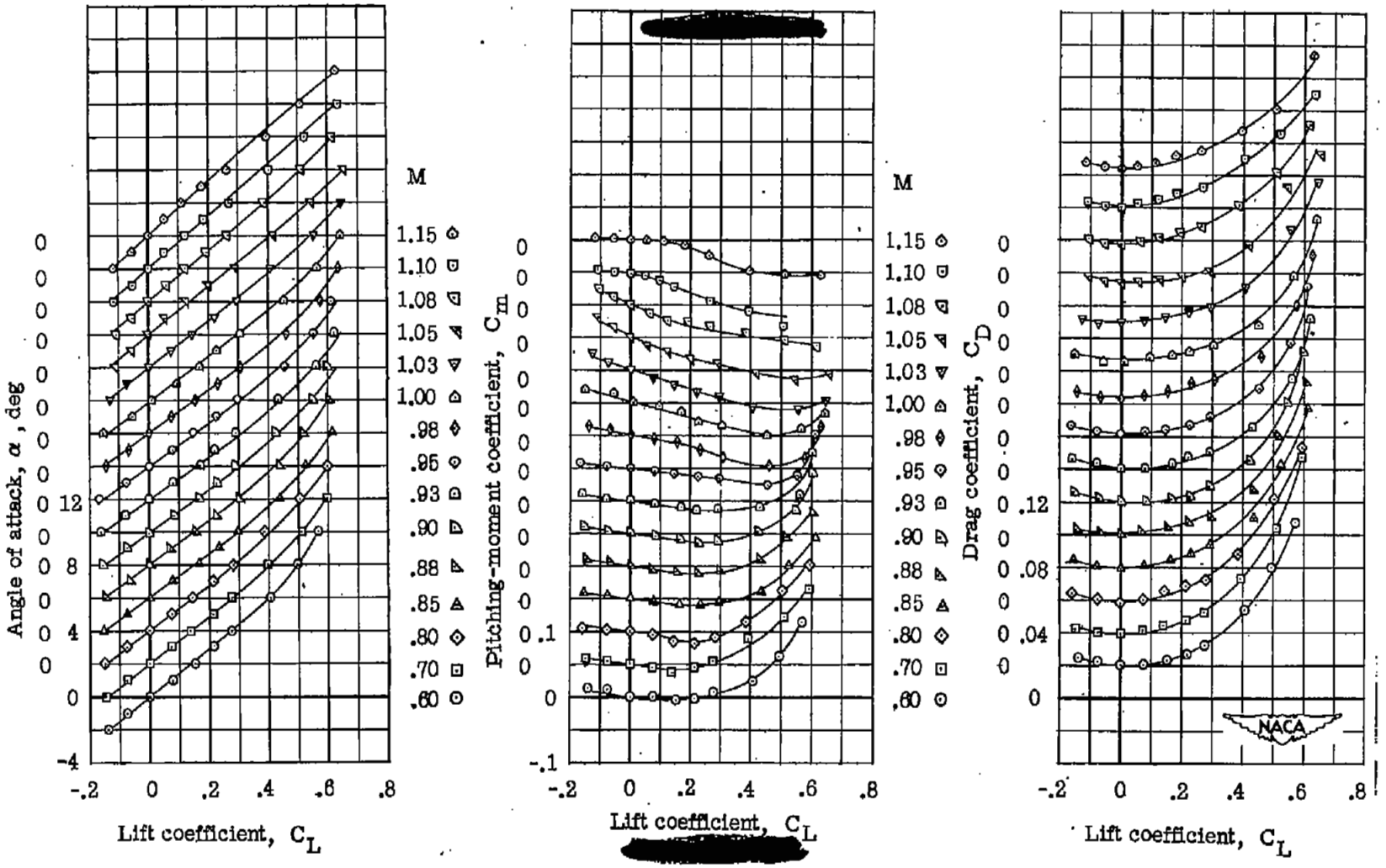

Figure 9.- Aerodynamic characteristics for a model with 45° sweptback wing, aspect ratio 6, taper ratio 0.6, and NACA 65A006 airfoil section. Wing fuselage.

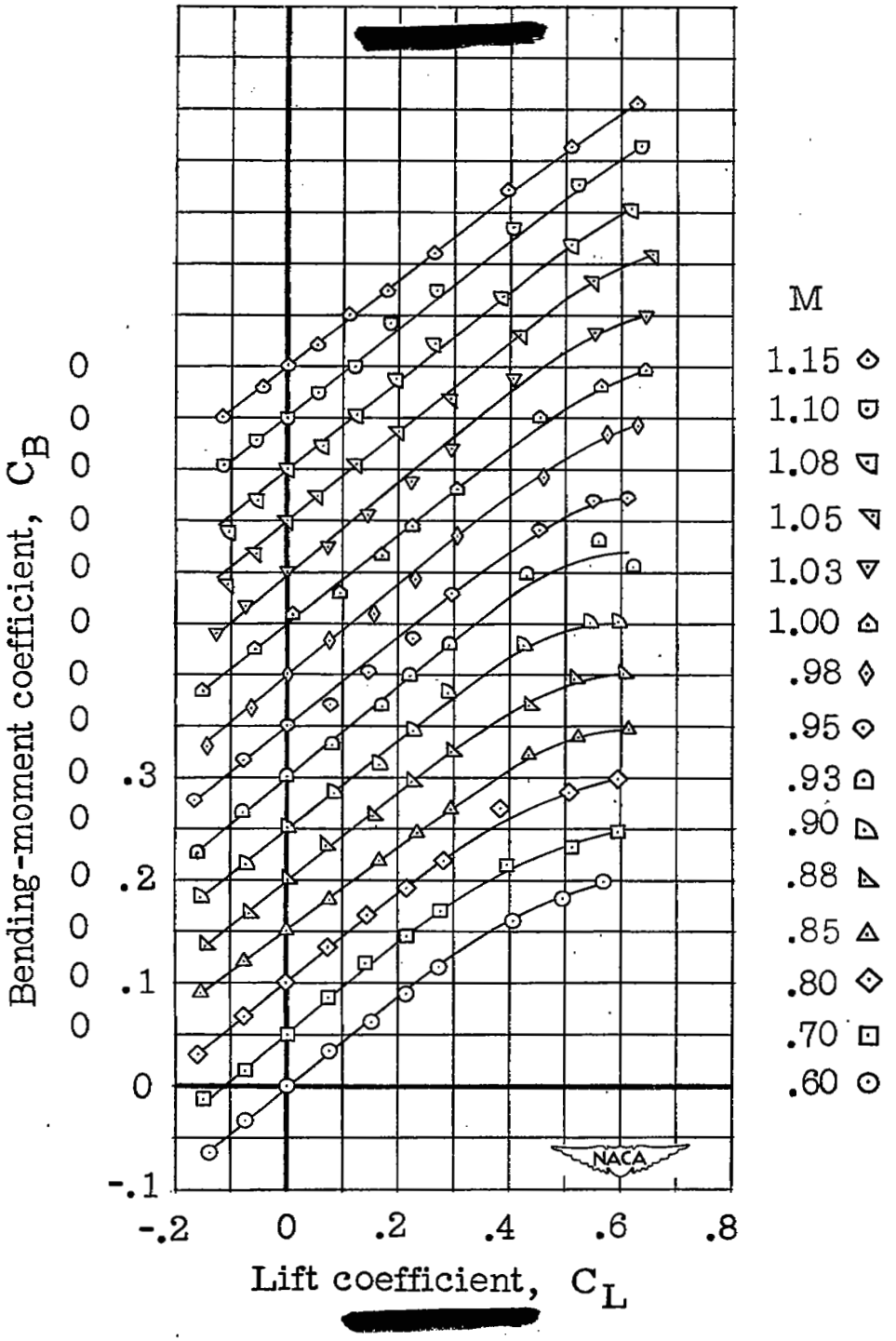

Figure 9.— Concluded.

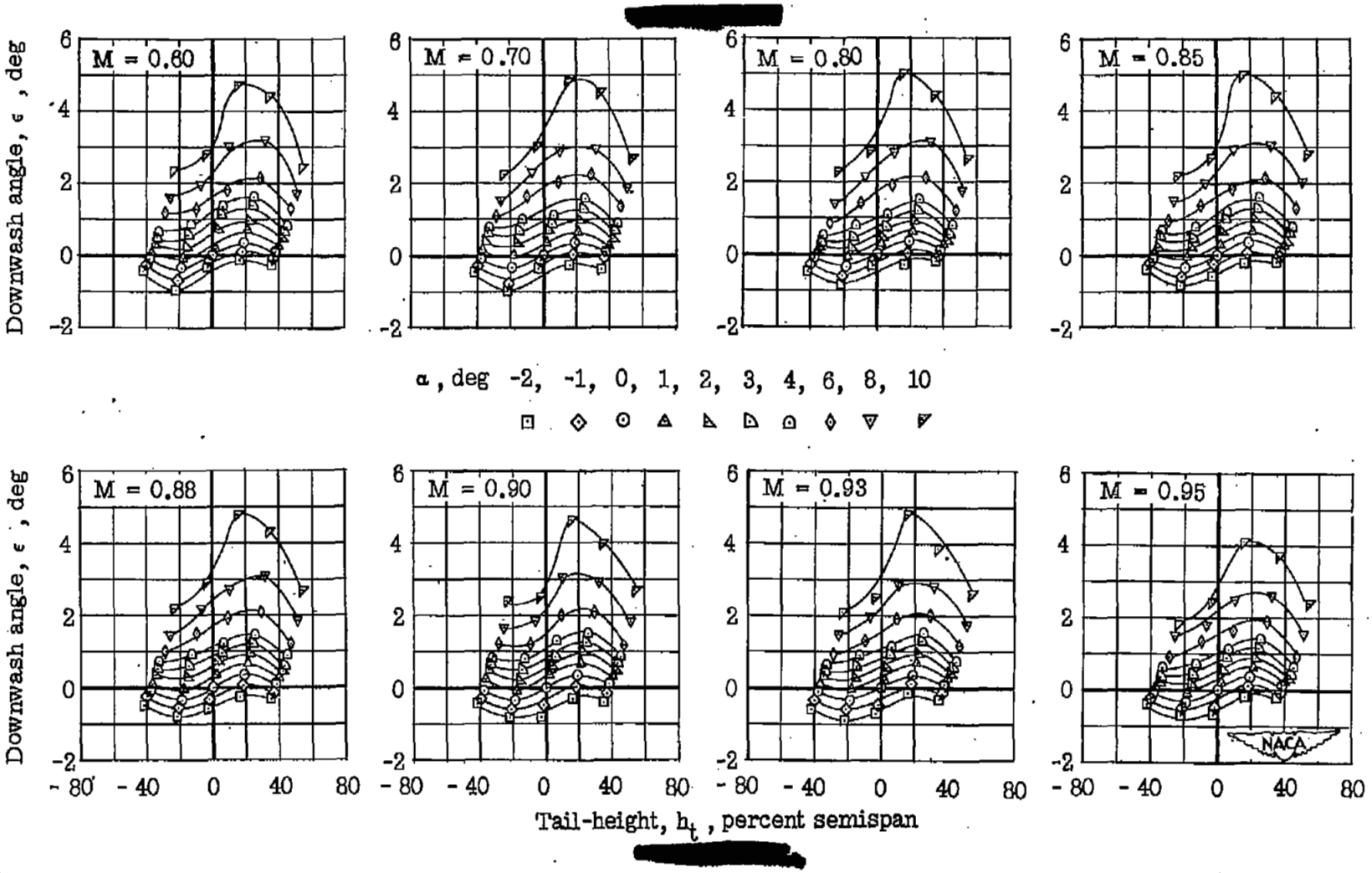

Figure 10.– Effective downwash angles in region of tail plane for a model with 45° sweptback wing, aspect ratio 6, taper ratio 0.6, and NACA 65A006 airfoil section. Wing alone.

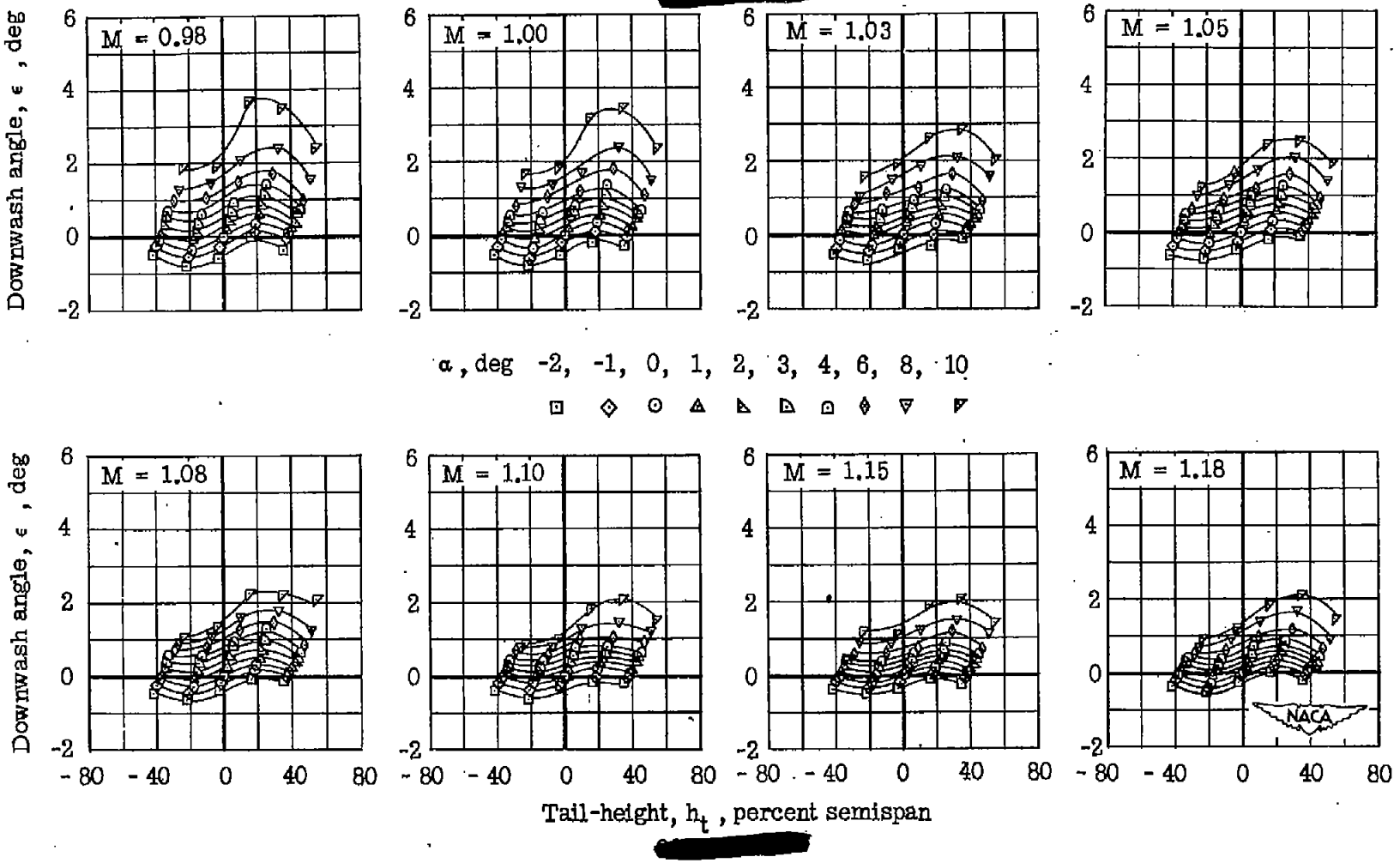

Figure 10.– Concluded.

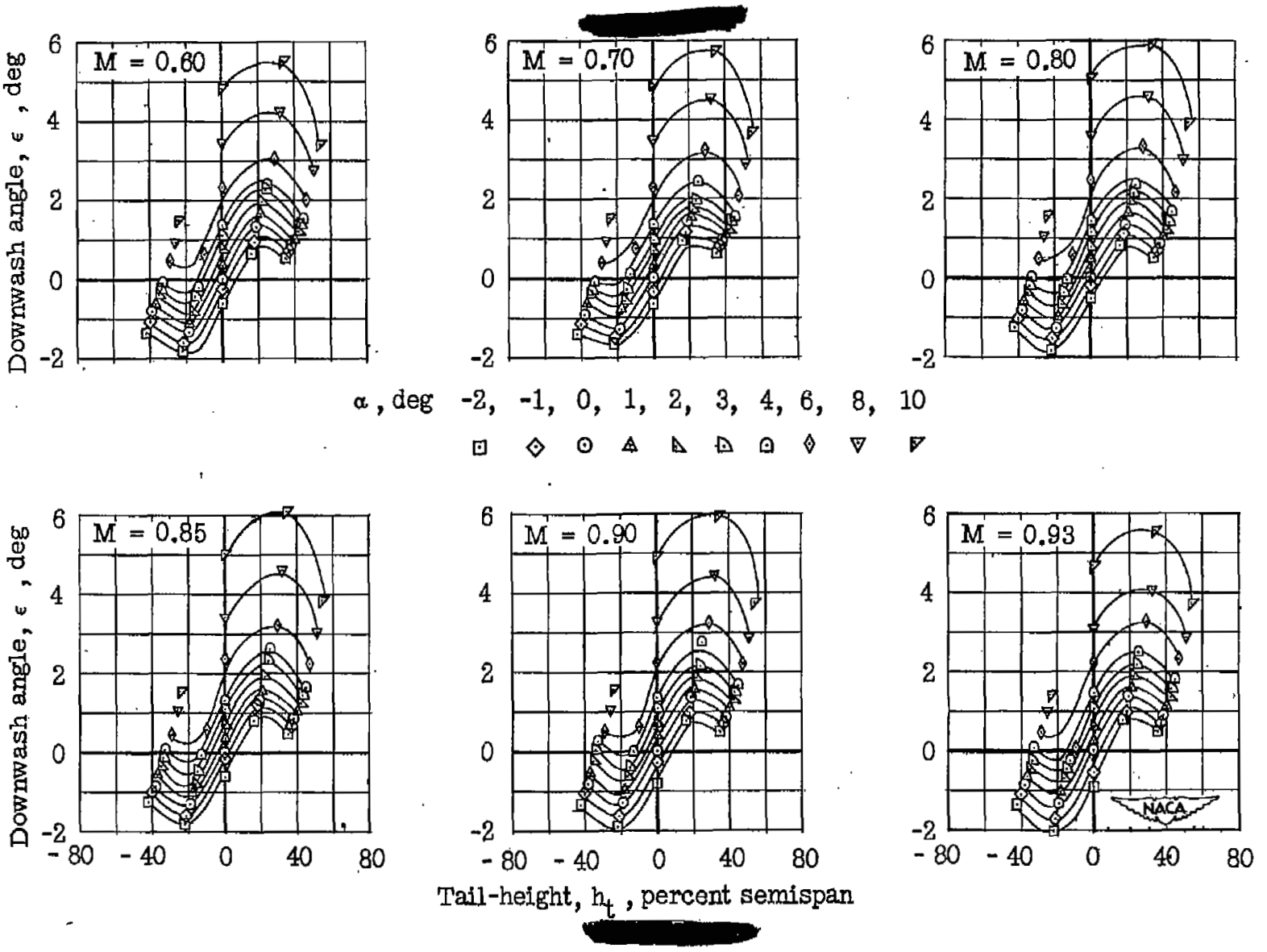

Figure 11.– Effective downwash angles in region of tail plane for a model with 45° sweptback wing, aspect ratio 6, taper ratio 0.6, and NACA 65A006 airfoil section. Wing fuselage.

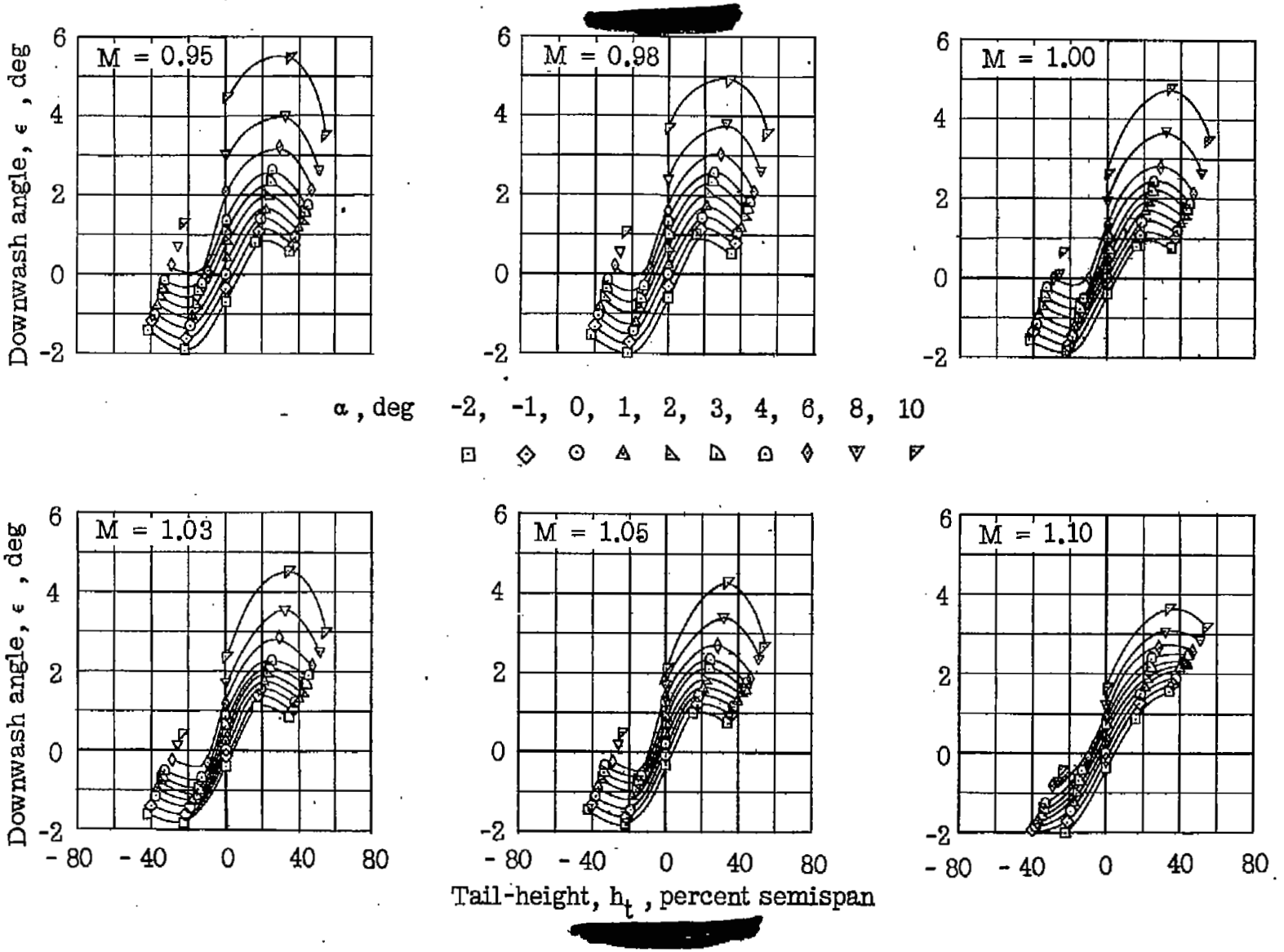

Figure 11.- Concluded.

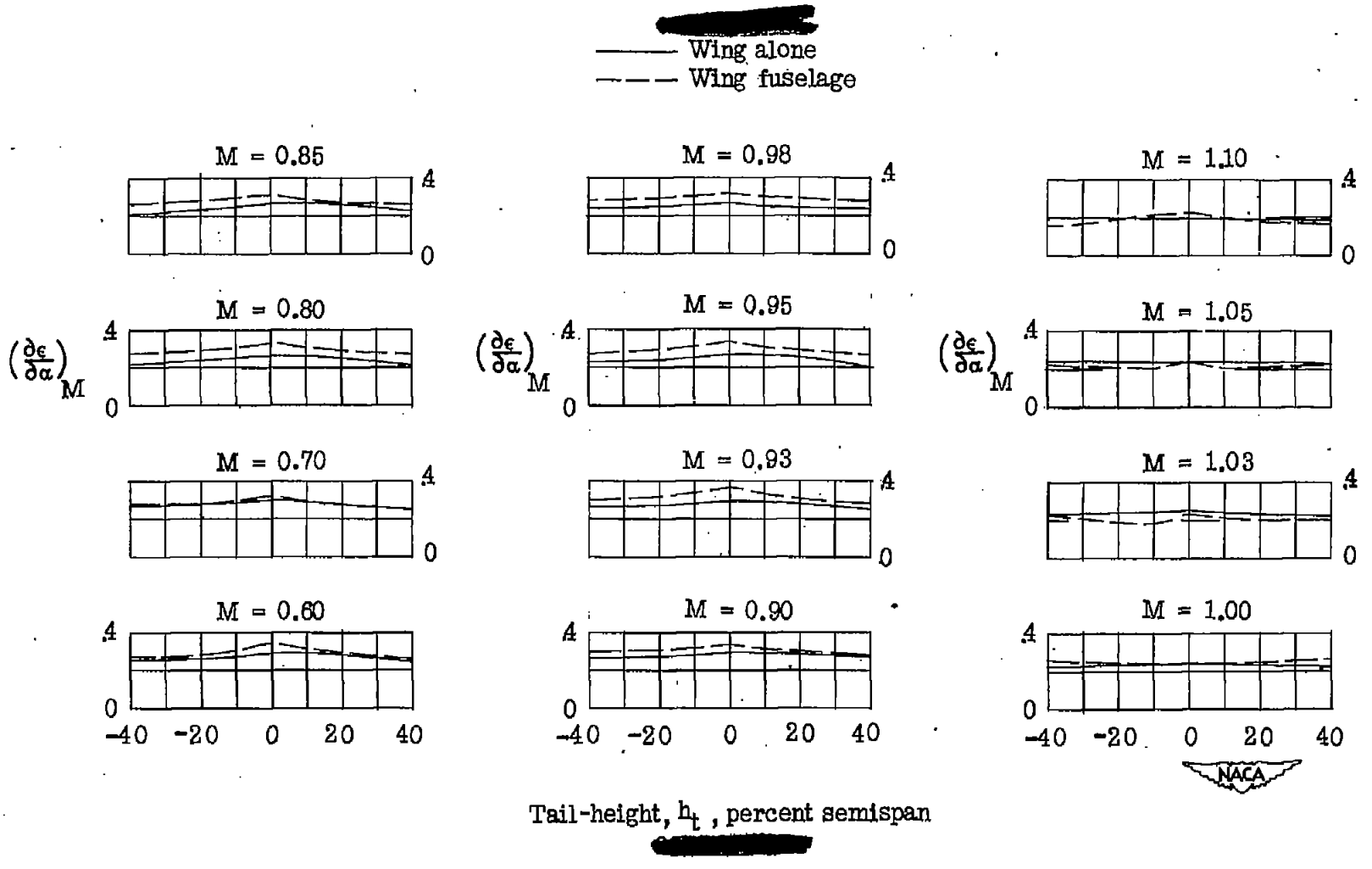

Figure 12.– Variation of downwash gradient with tail height and Mach number for a model with 45° sweptback wing, aspect ratio 6, taper ratio 0.6, and NACA 65A006 airfoil section. $C_L = 0$.

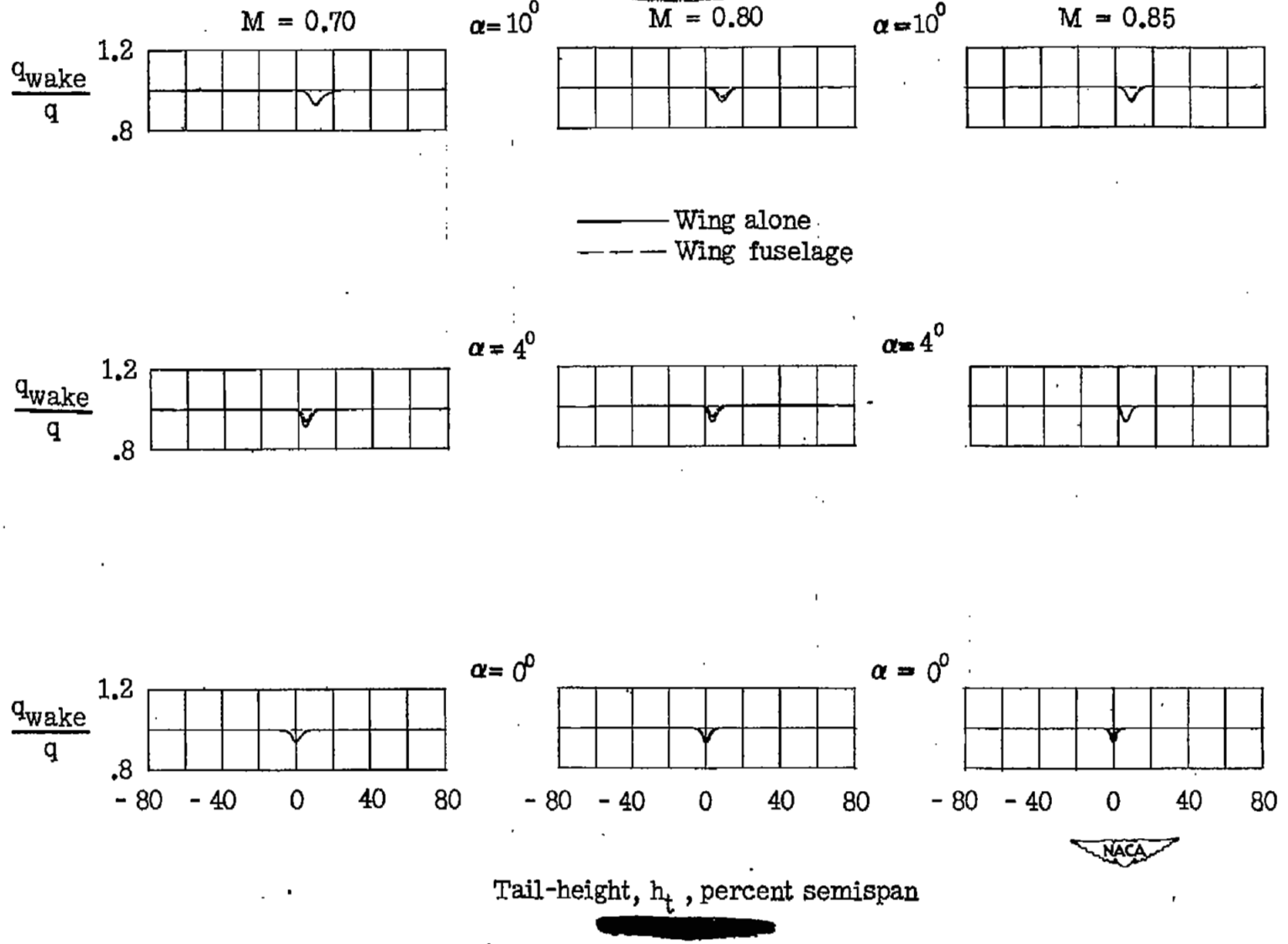

Figure 13.– Dynamic–pressure surveys in region of tail plane for a model with 45° sweptback wing, aspect ratio 6, taper ratio 0.6, and NACA 65A006 airfoil section.

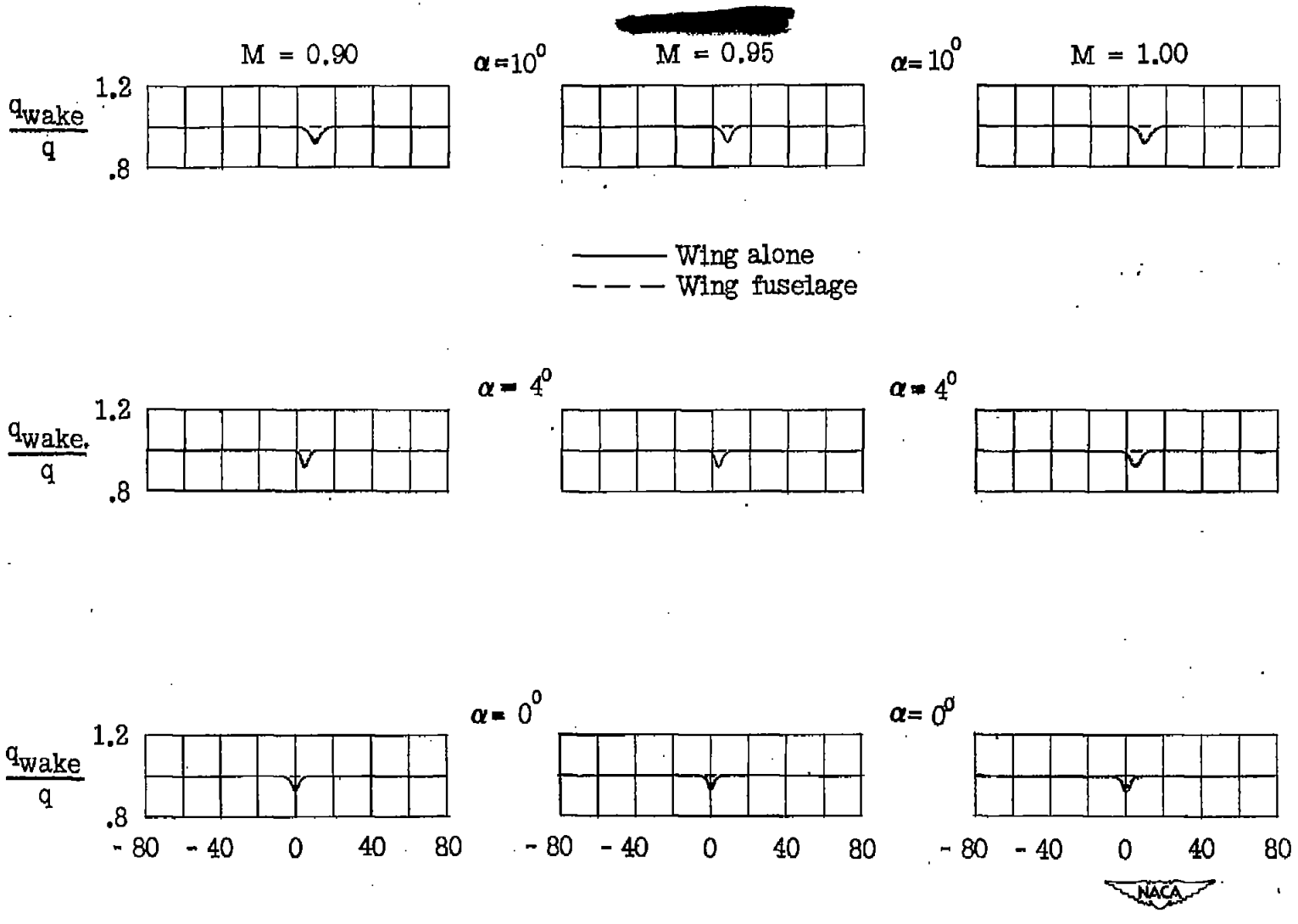

Figure 13.- Continued.

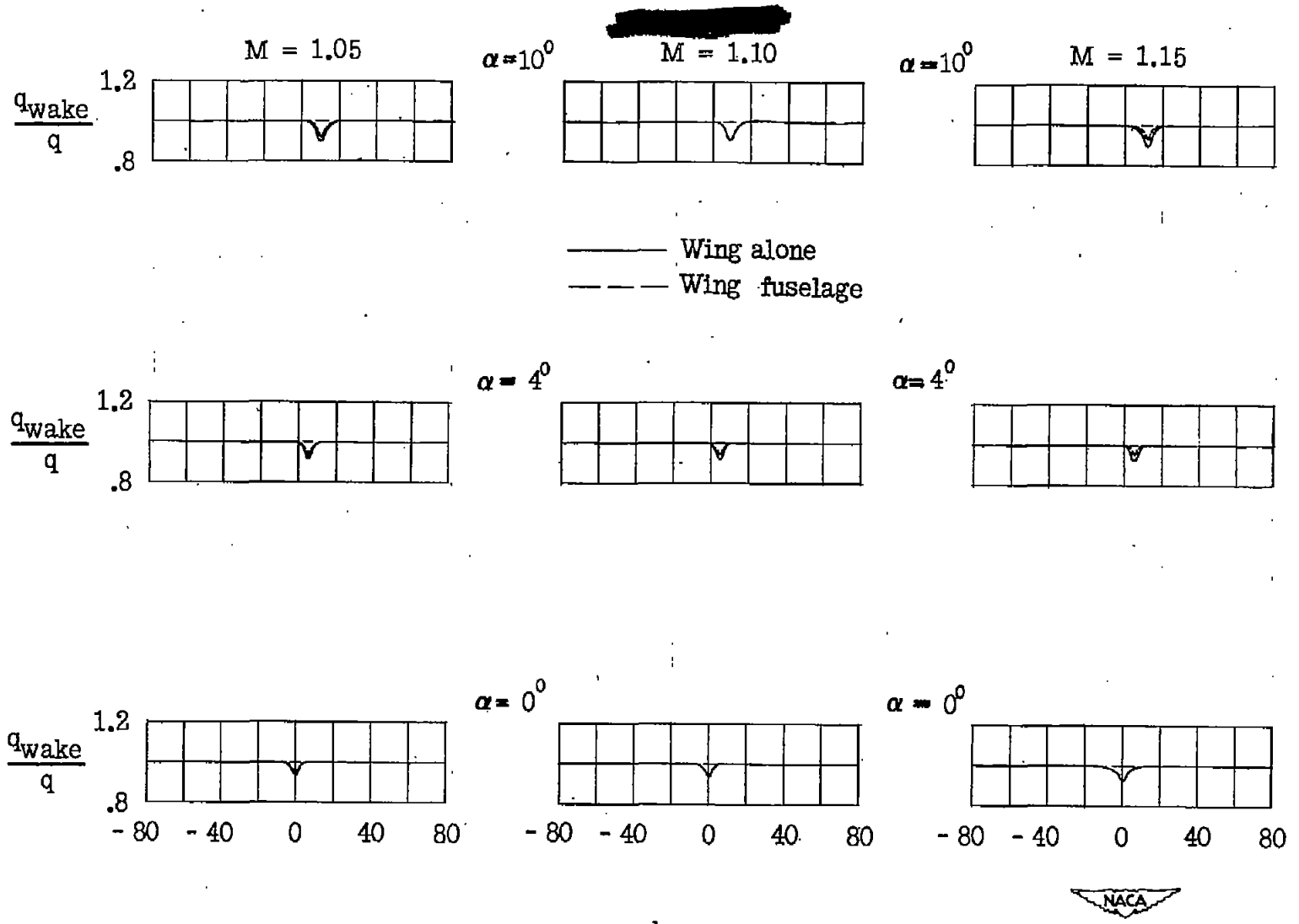

Figure 13.- Concluded.

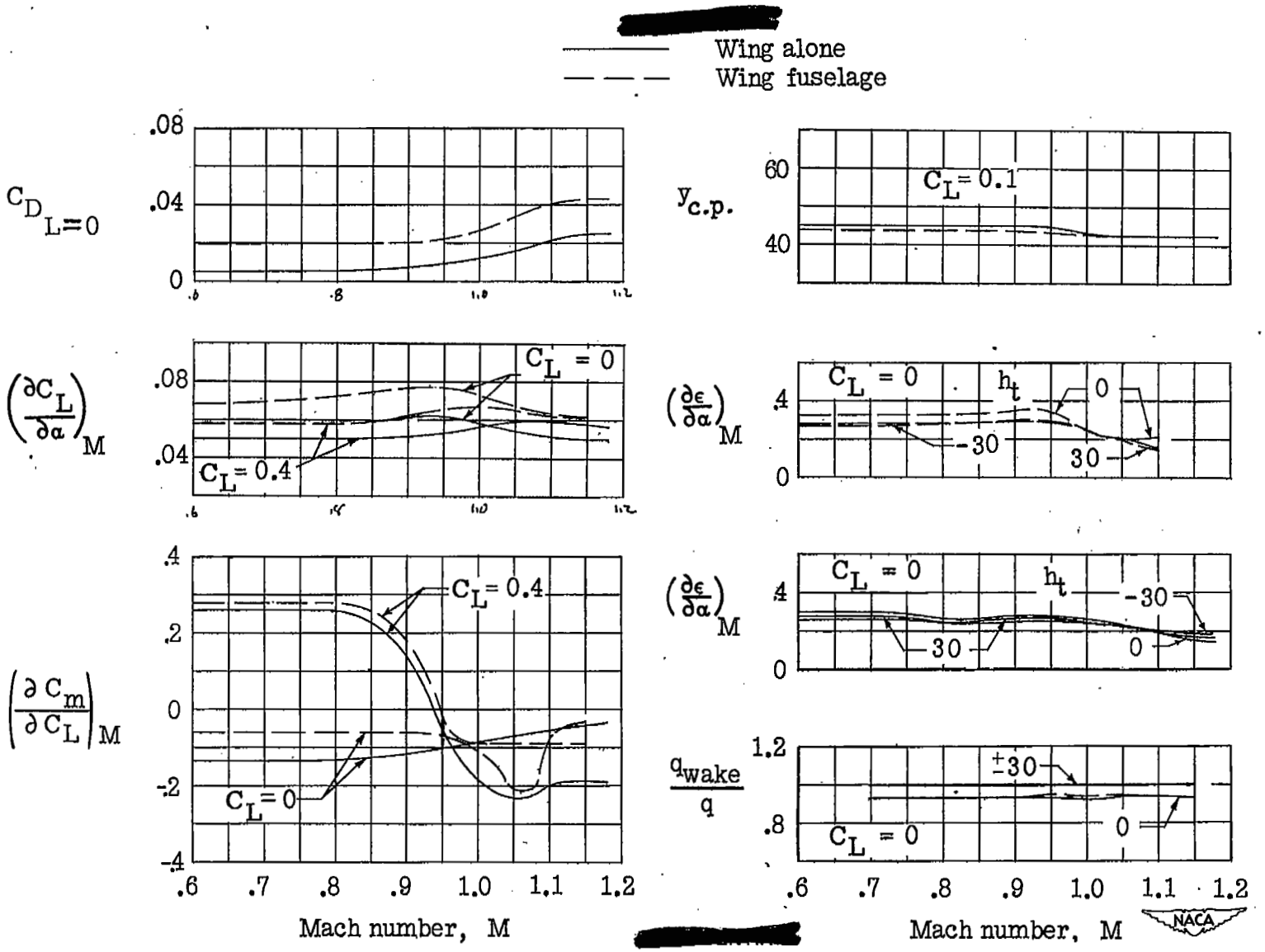

Figure 14.– Summary of aerodynamic characteristics for a model with 45° sweptback wing, aspect ratio 6, taper ratio 0.6, and NACA 65A006 airfoil section.

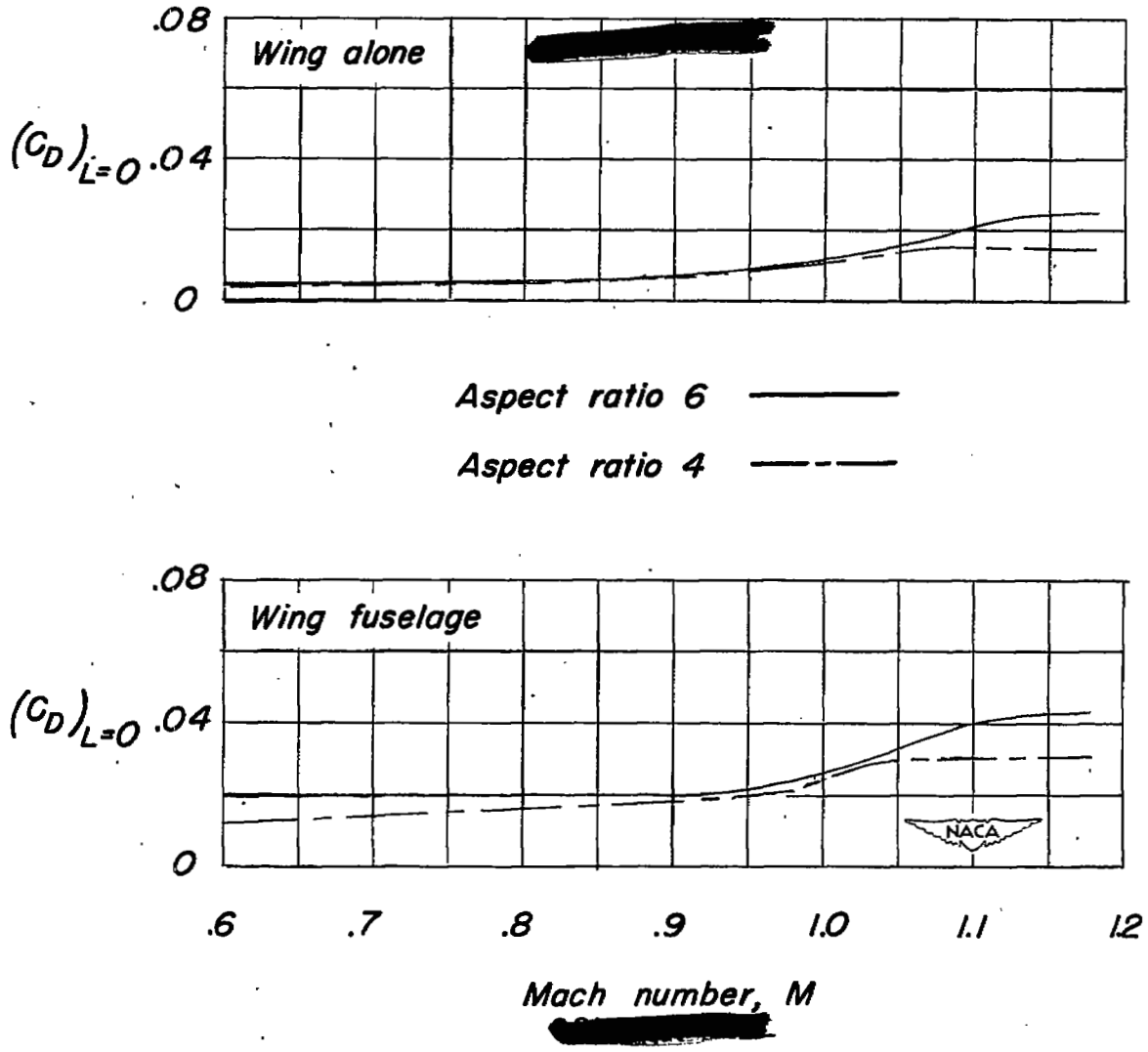

Figure 15.– Effect of aspect ratio on the minimum drag characteristics obtained from tests using a sponge–wiper seal for wings with 45° sweepback, taper ratio 0.6, and NACA 65A006 airfoil section.